Computation of Yield and Failure Surfaces for Biaxial Bending with Axial Force of Reinforced Concrete Sections with Jackets

M.G. Sfakianakis
University of Patras, Dept. of Civil Engineering, Greece

SUMMARY:
An existing fiber model for the study of the failure mechanism of reinforced concrete sections with arbitrary shape in biaxial bending with axial force is extended for the computation of yield and failure surfaces of RC sections when they are strengthened with RC jackets. In many nonlinear models for RC prismatic members the knowledge of the exact shape of those surfaces is critical for the needs of a reliable pushover analysis, where the plastic hinge formation is required for a given reinforced concrete framed structure. The procedure is based on an alternative fiber model which employees computer graphics as a computational tool for the integration of normal stresses over the section area. Thus, any numerical problems or large computer storage demands that are met in similar fiber models are fully eliminated. More over, the proposed fiber model can easily be incorporated into existing FEM codes for pushover nonlinear analysis.

Keywords: Bending, Fiber, Graphics, Failure, Jacket.

1. INTRODUCTION

The yield or failure surface of an arbitrary cross section in the axial load-bending moment components space N-M_y-M_z, can be defined as the geometrical locus of points (N,M_y,M_z) which correspond to the yield or ultimate strength (failure state) of the section, respectively. The result is closed surfaces which cannot be described by simple relationships of closed form, as those used for the classic orthogonal section (Fardis, 2009). These surfaces fully depend on the detailed section geometry, on the reinforcement amount and on the way it is placed inside the section. On the other hand, for the needs of nonlinear analysis, the detailed knowledge of those surfaces is extremely important since the plastic deformations of a structural element are functions of its load history and of the distance of its load vector from those surfaces. The problem becomes more complicated when the member sections are strengthened perimetrically with RC jackets, because of the existence of two different concrete qualities and/or two different steel qualities plus the composite section geometry. In this case, it is obvious that only the use of pure fiber models or those which divide the section into parallel to the neutral axis strips can produce numerically the exact shape and size of yield and failure surfaces. Among the most representative models found in the literature, which belong to the above categories but for unstrenghthened sections, one can report those of Al-Noury and Chen (1982), Cheng-Tzu and Hsu (1985), Sousa Jr and Muniz (2007), Charalampakis and Koumousis (2008).
In the present work, a fiber model based on computer graphics, which was initially developed by the author (Sfakianakis, 2002) for cross sections of arbitrary shape for the computation of the failure surface, is extended for the case of computation of the yield surface too, as well as the full moment-curvature diagrams considering or not a perimetrical RC jacket for the section. The original version of the model could handle the cases of orthogonal cross sections with or without jacket, cross sections of arbitrary shape but without jacket, and only for the computation of the failure surface. More over, the present version of the model incorporates significant algorithmic improvements which have to do with the fast computation of the neutral axis position in the section and the moment-curvature diagrams, for a specific value of the axial load N. Finally, representative examples are presented which show clearly the effectiveness of the model to produce accurate results for the section analysis either for the initial design or for seismic assessment of RC framed structures.

2. GEOMETRICAL DEFINITIONS

The initial cross section may be of arbitrary shape, convex or not. Perimetrically it is enclosed with a RC jacket of constant thickness t_j. Fig. 1 shows the geometry of such a section with the assumed strain profile and the stress-strain diagrams for the materials. For each material, concrete or steel, it is assumed that there exist two different qualities. Also, it is assumed a common linear strain profile for all the materials. This means that the Euler-Bernouli assumption is considered to be valid, as well as that there is not any relative slip in the intercace between the two concretes. Notation C2, C1, S2 and S1 in Fig. 1 refers to the most outer concrete (C) and steel (S) vertices of the initial cross section, nor-mally to the neutral axis, which are in tension (1) and compression (2) state. For the jacket section the previous indices are replaced by the points C2J, C1J, S2J and S1J.

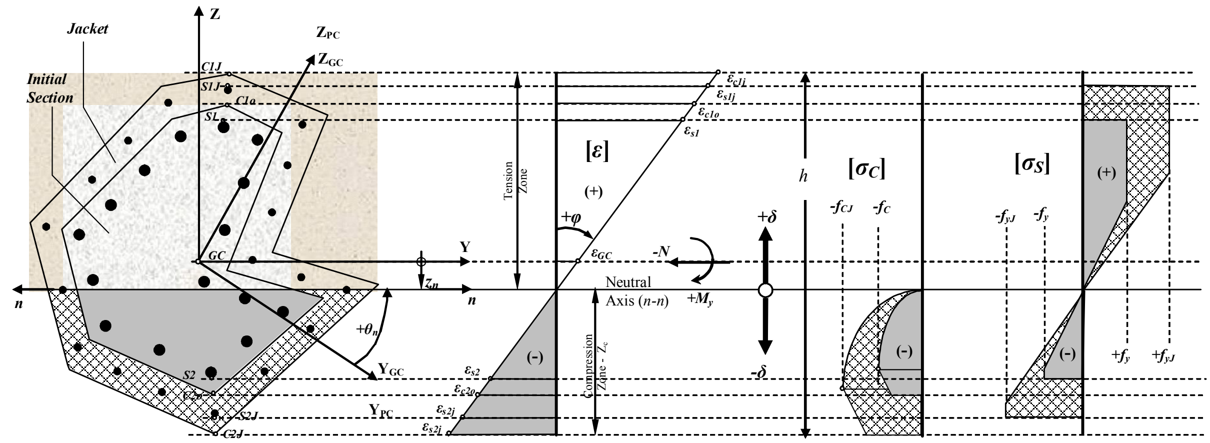

Figure 1. Section geometry, strain profile and material σ-ε diagrams.

The concrete area of a section is divided into two separate areas, (a) that of the concrete cover outside of the stirrup and (b) to that of the core inside the stirrup. The reason is that the model takes into account different compressive strengths for the two areas, f_c and f_c^* respectively, where f_c^* is the increased compressive strength due to confinement of the concrete by the stirrups. Fig. 2 shows the definition of the section core for an orthogonal cross section with and without jacket. According to various RC Codes (e.g. Eurocode 2, Greek EKOS-2000, FEMA 356, Greek KAN.ΕΠΕ. 2012, etc.) the core limits extend from the interior area of the section to the axis of the perimetric stirrup. Thus, for the orthogonal cross section of Fig. 2 without the jacket the core area is $A_{co} = b_o h_o$ where $b_o = b - 2c - \varnothing_h$ and $h_o = h - 2c - \varnothing_h$. In these relations c and $\varnothing_h$ are the clear concrete cover out of the stirrup and the stirrup diameter, respectively. Similarly, for the case with the section with jacket of thickness t_j, and after the removement of the initial concrete cover c, the jacket core area is $A_{coj} = b_{oj} h_{oj} - A_{co}$, with $b_{oj} = b - 2c_j - \varnothing_{hj}$, $h_{oj} = h - 2c_j - \varnothing_{hj}$, where c_j, $\varnothing_{hj}$ are referred to the jacket, see Fig. 1. As mentioned before, the model assumes separate compressive strengths for cover and core areas. For the case of jacket it is able to assume a unique jacket core area of dimensions $A_{coj} = b_{oj} h_{oj}$ and compressive strength f_{cj}^*, or two different cores $A_{coj} = b_{oj} h_{oj} - A_{co}$ and $A_{co} = b_o h_o$ with compressive strengths f_{cj}^* and f_c^* respectively. In this point it is worthnoting that there are not any extensive experimental data to clarify which assumption is more valid. The second assumption is more conservative and is obvious that gives a little reduced bending strength of the section in comparison with the first one.
The above geometrical definitions and the compressive strength assumptions, as mentioned for the orthogonal cross section, are valid for any arbitrary cross section shape.

3. COMPUTER GRAPHIC FIBER MODEL

The present fiber model uses computer graphics as a computational tool for the discretization of the cross section into fibers. More specific, the fibers are the pixel elements of the computer monitor. For

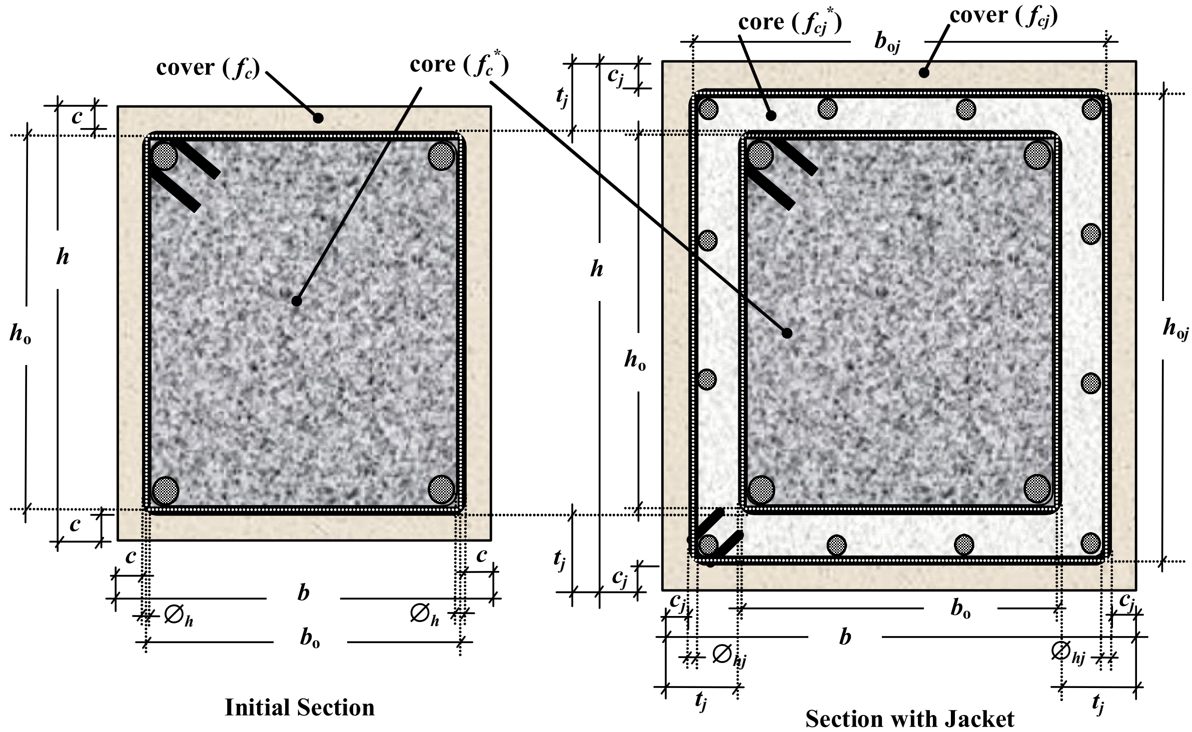

Figure 2. Core definition in an orthogonal section with and without jacket.

this purpose the section is designed in the monitor with a desired scale using different color per each material (concrete or steel) and per each material area (concrete cover or core and steel of original section or that of the jacket). In this way the whole section is considered to consist of horizontal "ribbons" of pixels parallel to the graphic window horizontal axis, as shown in Fig. 3.

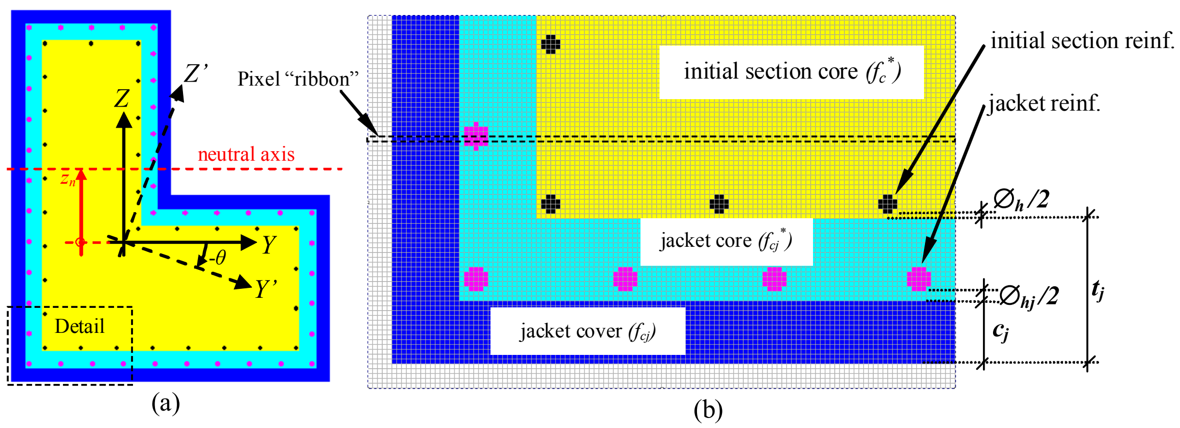

Figure 3. Sample of a pixel grid map of a section: (a) L section with jacket, and (b) magnified detail.

As an example, consider the orientation of the L section of Fig. 3. The obtained color picture on the monitor is scanned (optical recognition) ribbon-by-ribbon retaining for each pixel its own color, for recognizing the kind of the material, and its coordinates (y,z) on the centroid Cartesian system Y-Z. The pixels of a specific ribbon have common z coordinate and are under the same strain value ε. Because of this fact, the square shape of the pixels and of their extreme small dimensions (e.g. 0.29 mm for a 19" monitor with 1280×2024 resolution), they can be considered as almost dimensionless areas (≈ points) with the same stress value σ for each material. Hence, for each ribbon, during the scanning process, the position of the resultant force of each material is being computed simply by

taking area moments about the Z axis. Finally, for each ribbon the y-coordinate of the resultant force of each material, the common z-coordinate and the number of pixels per material are kept in different one-dimensional arrays. In this way the overall cross section problem is reduced to a problem of concentrated points at specific locations (y,z) and specified stress σ, strain ε and area A.
The full yield or failure surfaces in the Cartesian space N-M_y-M_z of a section are constructed assuming all the possible values of the angle θ between the neutral axis and the Y centroidal axis in the range (0^o, 360^o). It is obvious that the above optical recognition procedure requires the neutral axis to be always horizontal, so the section is rotated in angles of $-\theta$ in the above range at predefined steps $d\theta$. The centroid system Y-Z takes a new orientation Y'-Z', so the obtained (y,z) coordinates of each ribbon and material, must be transformed to (y',z'). Fig. 4 shows the positions of the resultant forces for each horizontal pixel-ribbon and for each material for the L cross section of Fig. 3 for $\theta = 30^o$.

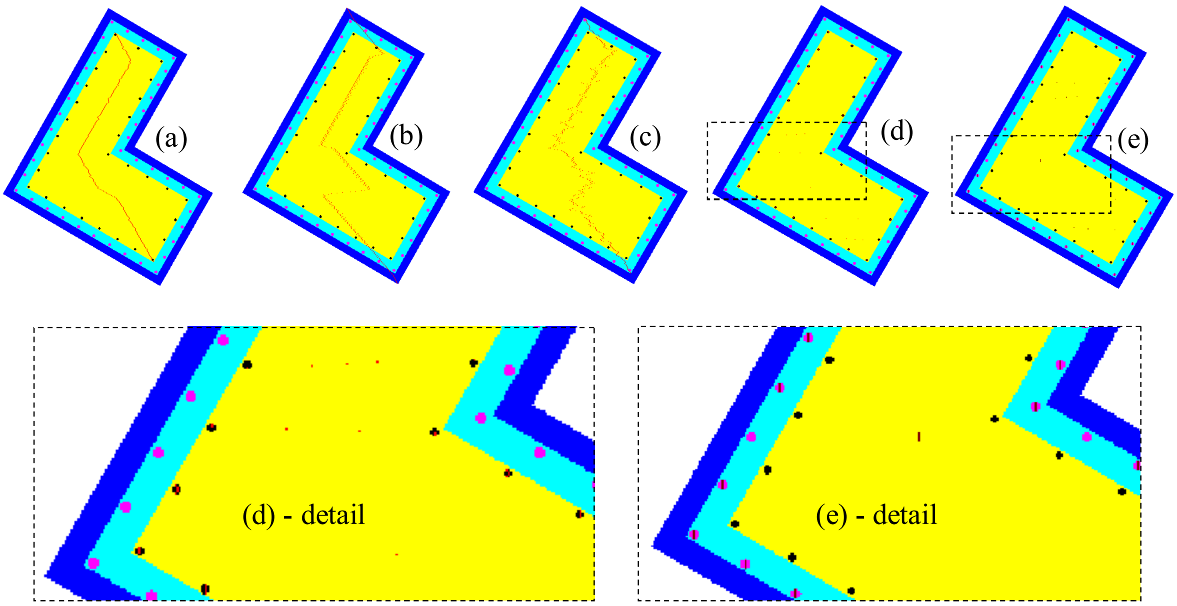

Figure 4. Position of ribbon resultant forces for: (a) initial section concrete core, (b) jacket concrete core, (c) jacket concrete cover, (d) initial section reinforcement, and (e) jacket reinforcement.

From this point and on, for a specific location z_n and angle θ of the neutral axis (see Fig. 3) and for an imposed value of curvature φ around the neutral axis, the internal section forces and moment components can be easily computed by the known integrals which take the following form for the section pixel fibers.

$$\begin{aligned} N_{\text{int}} &= N_{cj} + N_{coj} + N_{co} + N_{sj} + N_s = \\ &= \int_{A_{cj}} \sigma_{cj}(y,z)dA_{cj} + \int_{A_{coj}} \sigma_{coj}(y,z)dA_{coj} + \int_{A_{co}} \sigma_{co}(y,z)dA_{co} + \sum_{i=1,}^{n_{sj}} a_{sj,i}\sigma_{sj,i} + \sum_{i=1,}^{n_s} a_{s,i}\sigma_{s,i} = \\ &= dy^2\left(\sum_{i=1}^{i=r} n_{cj,i}\sigma_{cj,i} + \sum_{i=1}^{i=r} n_{coj,i}\sigma_{coj,i} + \sum_{i=1}^{i=r} n_{co,i}\sigma_{co,i} + \sum_{i=1}^{i=r} n_{sj,i}\sigma_{sj,i} + \sum_{i=1}^{i=r} n_{s,i}\sigma_{s,i}\right) \end{aligned} \tag{3.1}$$

$$\begin{aligned} M_{y,\text{int}} &= M_{y,cj} + M_{y,coj} + M_{y,co} + M_{y,sj} + M_{y,s} = \\ &= \int_{A_{cj}} z\sigma_{cj}(y,z)dA_{cj} + \int_{A_{coj}} z\sigma_{coj}(y,z)dA_{coj} + \int_{A_{co}} z\sigma_{co}(y,z)dA_{co} + \sum_{i=1,}^{n_{sj}} z_{sj,i}a_{sj,i}\sigma_{sj,i} + \sum_{i=1,}^{n_s} z_{s,i}a_{s,i}\sigma_{s,i} = \\ &= dy^2\left(\sum_{i=1}^{i=r} z_{cj,i}n_{cj,i}\sigma_{cj,i} + \sum_{i=1}^{i=r} z_{coj,i}n_{coj,i}\sigma_{coj,i} + \sum_{i=1}^{i=r} z_{co,i}n_{co,i}\sigma_{co,i} + \sum_{i=1}^{i=r} z_{sj,i}n_{sj,i}\sigma_{sj,i} + \sum_{i=1}^{i=r} z_{s,i}n_{s,i}\sigma_{s,i}\right) \end{aligned} \tag{3.2}$$

$$
\begin{aligned}
M_{z,\text{int}} &= M_{z,cj} + M_{z,coj} + M_{z,co} + M_{z,sj} + M_{z,s} = \\
&= \int_{A_{cj}} y\sigma_{cj}(y,z)dA_{cj} + \int_{A_{coj}} y\sigma_{coj}(y,z)dA_{coj} + \int_{A_{co}} y\sigma_{co}(y,z)dA_{co} + \sum_{i=1,}^{n_{sj}} y_{sj,i}a_{sj,i}\sigma_{sj,i} + \sum_{i=1,}^{n_s} y_{s,i}a_{s,i}\sigma_{s,i} = \\
&= dy^2\left(\sum_{i=1}^{i=r} y_{cj,i}n_{cj,i}\sigma_{cj,i} + \sum_{i=1}^{i=r} y_{coj,i}n_{coj,i}\sigma_{coj,i} + \sum_{i=1}^{i=r} y_{co,i}n_{co,i}\sigma_{co,i} + \sum_{i=1}^{i=r} y_{sj,i}n_{sj,i}\sigma_{sj,i} + \sum_{i=1}^{i=r} y_{s,i}n_{s,i}\sigma_{s,i}\right)
\end{aligned} \tag{3.3}
$$

In the above relations indices c, co, s and j correspond to concrete cover, concrete core, steel and jacket, respectively, while r is the total number of pixel-ribbons of the section and n is the number of pixels of each ribbon. If A is the total area of the section, then the equivalent area of each pixel is dy^2, with $dy = \sqrt{A/n_{tot}}$ and n_{tot} being the total number of color pixel-fibers of the section. Further computational details about the material stress-strain laws $\sigma(\varepsilon)$ can be found in Sfakianakis (2002).

4. CONSTRUCTION OF YIELD AND FAILURE SURFACES

The construction of the yield or failure surface by the present fiber model consists of the computational steps described below. All geometric parameters are shown in Fig. 1.

Step 1.
Selection of the yield or failure criterion. For this purpose we choose as control fibers the pairs (ε_{c2},ε_{s1}) or (ε_{c2o},ε_{s1}). The first one corresponds to yield or failure of the most outer compressive concrete fiber of the section in relation to the yield or failure of the most outer reinforcement bar which is in most tension condition. The yield or failure state is defined when at least one of the two fibers of the selected pair reaches first its strain limit ε, as it is defined by the RC Codes. The second pair works exactly as the first one but the concrete control fiber is that of the jacket core.
For the yield surface the corresponding strain limits for the two pairs are (ε_{cy},ε_{sy}), which are the yield strains for concrete and steel, respectively. For the failure surface the strain limits are (ε_{cu},ε_{su}) which are defined as the strains at the ultimate strength of each material.

Step 2.
Since the surfaces are constructed meridian by meridian, we choose the angle θ of a specific meridian from the range (0^o,360^o) using predefined steps $d\theta$. It is noted that in general the meridians are not plane. In other words $\theta_n \neq \tan^{-1}(M_z/M_y)$. This is due to secondary moments that may occur about an axis which is perpendicular to the neutral axis, and passes through the origin of the section Cartesian system *Y-Z*. These secondary moments about this axis may happen because of possible variations of concrete and/or steel stresses from both sides of the axis. As will be shown clearly in the examples, this variation depends on the unsymmetry of the cross section and on any unsymmetric distribution of the longitudinal reinforcement bars too.
A second data that must be selected is the axial load range for which the meridian will be computed step by step, as well as the axial load increment dN, so that $N_{k+1} = N_k + dN$. The full meridian corresponds to axial load limits N^+ and N^- as defined by the RC Codes.

Step 3.
For a specific value of an external axial load N_k, applied on the section, define two adjacent neutral axis positions $z_{n,1}$ and $z_{n,2}$, and corresponding curvatures φ_1 and φ_2, which give internal axial load values $N_{int,1}$ and $N_{int,2}$ such as $N_{int,1} \leq N_k \leq N_{int,2}$. These values must correspond to yield or failure of at least one fiber of the selected control fibers of step 1. Thus, for determining value $N_{int,1}$, set $\varepsilon_{c2} = \varepsilon_{cy}$ or ε_{cu} for yield or failure state, respectively, and $\varepsilon_{s1} = \varepsilon_{sy}$ or ε_{su}. From this strain profile compute $z_{n,1}$ and φ_1 and from Eqn. (3.1) the internal axial load value $N_{int,1}$. After this, keep ε_{c2} constant and compute $N_{int,2}$ changing only the values of z_n or φ, until finding a pair ($z_{n,2}$,φ_2) for which $N_k \leq N_{int,2}$. The procedure is repeated by successive bisections of the range ($N_{int,1}$,$N_{int,2}$) until $N_{int,1} = N_k$ or $N_{int,2} = N_k$. In this way the yield or failure of the section occurs when the most extreme compressive concrete fiber reaches first

its limit value $\varepsilon_{c2} = \varepsilon_{cy}$ or ε_{cu}, for yield or failure respectively, while the strain of the most outer bar in tension is still $\varepsilon_{s1} \leq \varepsilon_{sy}$ or ε_{su}.
On the other hand, the increase or decrease for first time the values of z_n or φ, leads to $N_{int,2} \leq N_{int,1} \leq N_k$ or $N_k \leq N_{int,1} \leq N_{int,2}$, then the procedure must start from the beginning keeping $\varepsilon_{s1} = \varepsilon_{sy}$ or ε_{su} constant, and changing ε_{c2} through the change of z_n or φ. This is the case where the yield or failure of the section occurs when the strain of the most outer bar in tension reaches first its limit value $\varepsilon_{s1} = \varepsilon_{sy}$ or ε_{su}, respectively, while the strain of the most extreme compressive concrete fiber is still $\varepsilon_{c2} \leq \varepsilon_{cy}$ or ε_{cu}.

Step 4.
For the strain profile of step 3, which fulfills the condition $N_k = \mathrm{N}_{int}$, using Eqn. (3.2) and (3.3) compute the moments components M_y and M_z.

Step 5.
Repeat steps 3 and 4 for the next value of axial load, N_{k+1}, from its desired range as defined in step 2.

Step 6.
Repeat steps 2 to 5 for the next value of angle θ, from its desired range as defined in step 2.

Referring to step 3, the above procedure can be significantly accelerated for a next value of the axial load N_{k+1}, if keep as $(N_{int,1}, z_{n,1}, \varphi_1)$ the values for which convergence occurred for the current value N_k. In a similar way, as increments of $dz_{n,2}$, or $d\varphi_2$ for finding $N_{int,2}$, one can use those of the current value N_k as a good initial approximation. In this way the range $(N_{int,1}, N_{int,2})$ is the smallest one, which in turn needs the less number of bisections until finding N_{k+1}, and so on.
The above modifications have been incorporated in a new version of the BIAX software, which was originally developed for the present graphics fiber model. Similar algorithmic improvements, the description of which is beyond the aim of this paper, have been made for the construction of the moment-curvature diagrams M-φ.

5. NUMERICAL EXAMPLES

5.1. Example 1

This example concerns the L-shaped column section of Fig. 5, with a constant jacket thickness $t_j = 94$ mm measured from the axis of the stirrup of the initial section. The initial section was designed by the

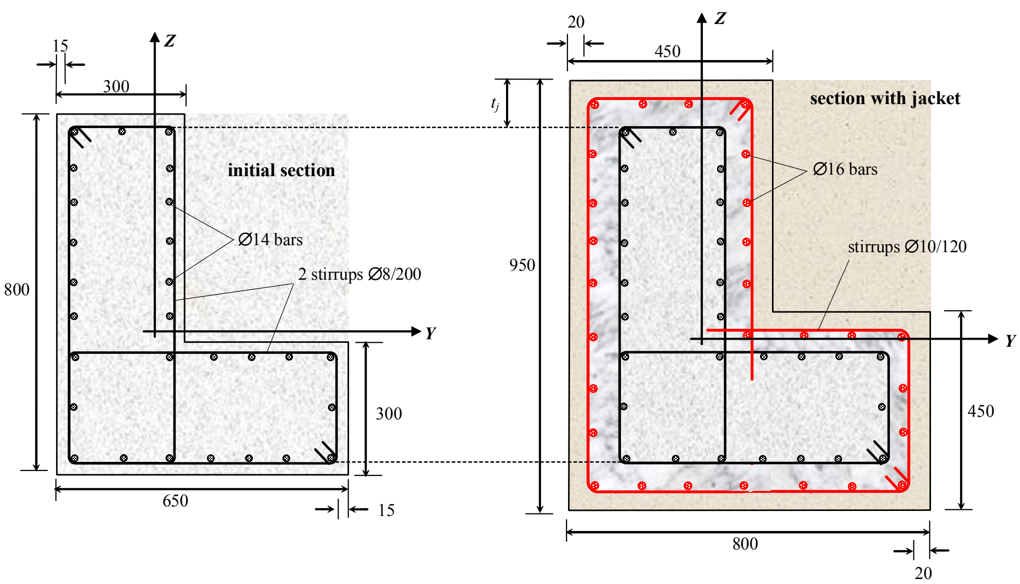

Figure 5. RC L-shaped section with jacket (dimensions in mm).

Old Greek National Code for Seismic Actions (1959) and it refers to a column section of a 3-story building. The strengthening of the section with RC jacket comes from the need of adding two more stories to the building. The material properties and safety factors used for the two sections of Fig. 5 are summarised in table 1 and correspond to design procedure according to Eurocode 2.

Table 5.1. Material properties and safety factors for the L-shaped sections of Fig. 5.

Section	f_c (MPa)	β_c	γ_c	ε_{co}	ε_{cu}	z	$\alpha\omega_w$	E_s (GPa)	f_y (MPa)	γ_s	ε_{su}
Initial	12	0.85	1.50	-0.002	-0.0035	0	0	200	220	1.15	0.020
Jacket	20	0.85	1.50	-0.002	-0.0035	0	0	200	500	1.15	0.020

In the above table, z is the slope of the descending branch of the concrete σ-ε law, which for design purposes is zero. Product α times ω_w expresses the confinement of the section core(s) by the stirrups. In this example this effect is neglected. The present graphics fiber model is used to produce the complete yield and failure surfaces of these sections using increments $\Delta\theta_n = 15^o$ for the rotation of the neutral axis. Fig. 6 and 7 shows these surfaces, in the normalized space ν-μ_y-μ_z, constructed meridian by meridian for the initial section and for that with the jacket, respectively. From the perspective views of these figures, the effect of the secondary moments, as they defined previously, is obvious since it gives non planar meridians.

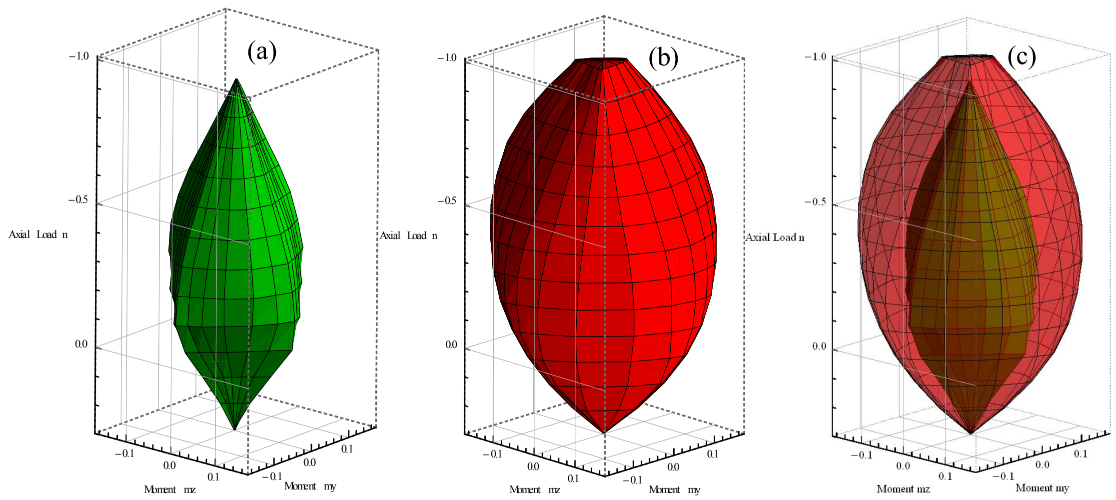

Figure 6. Yield and Failure surfaces of initial section: (a) Yield, (b) Failure, and (c) both, enclosed.

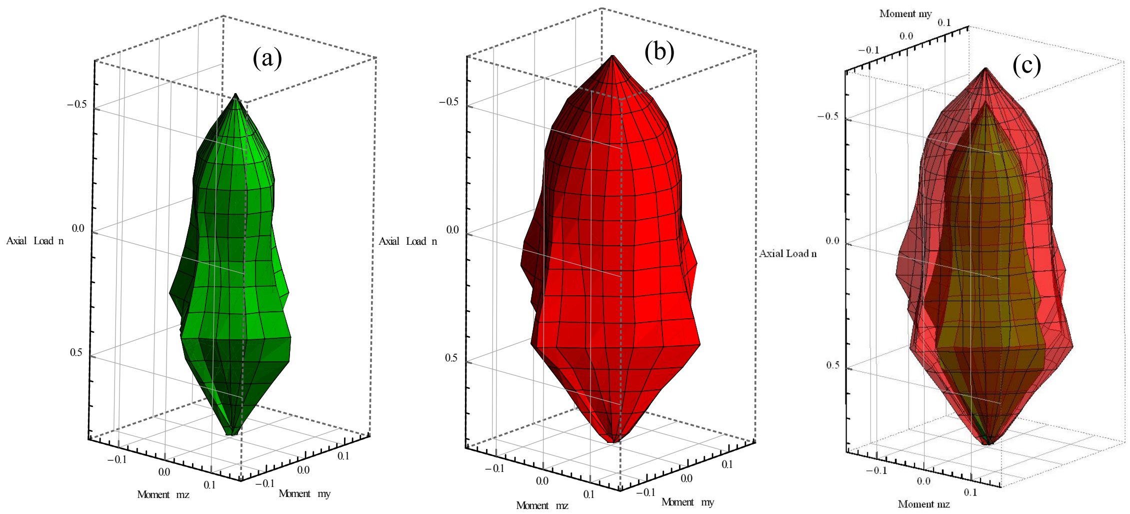

Figure 7. Yield and Failure surfaces of section with jacket: (a) Yield, (b) Failure, and (c) both, enclosed.

Notice that the surfaces of section with jacket are nonconvex in various regions. Fig. 8(a) shows clearly this property by presenting normalized values of isoload contours of the above surfaces in the tension range $v = (0.00,+0.20)$. Moreover, Fig. 8(b) shows that the surface meridians corresponding to neutral axis angle $\theta = 45^{o}$ are not planar because of the difference between angles $\alpha = \tan^{-1}(\mu_z/\mu_y)$ and θ (secondary moments effect).

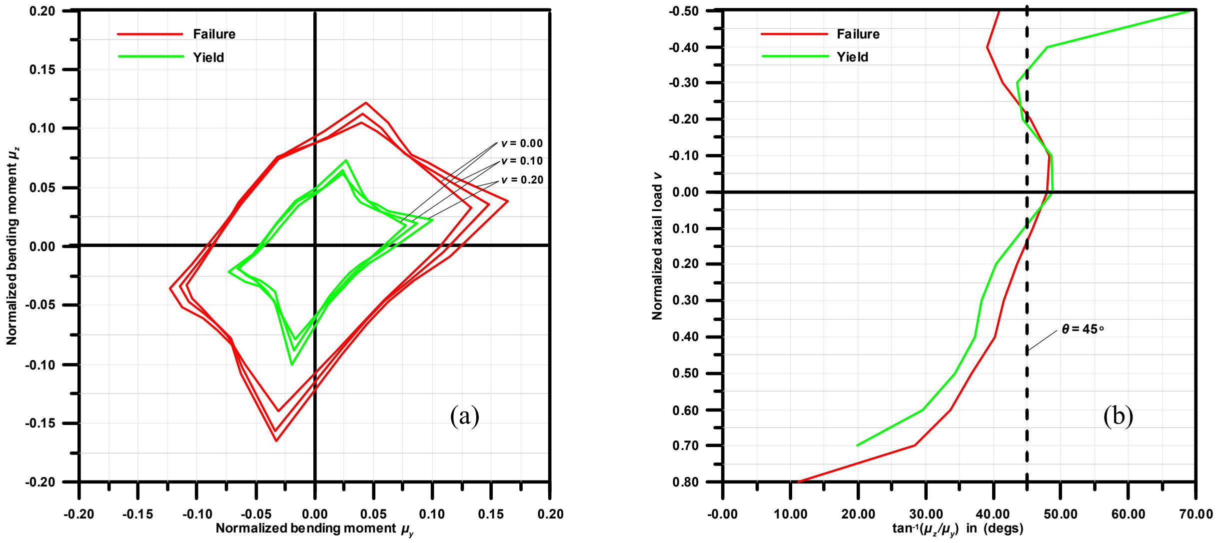

Figure 8. (a) Surface equators, and (b) moment component angle for $\theta = 45^{o}$.

5.2. Example 2

In this example the yield and failure surfaces are constructed for the nonsymmetric T-shaped column section of Fig. 9, with a constant jacket thickness $t_j = 69$ mm measured from the axis of the stirrups of the initial section. The initial column section belongs to the same building of example 1. The surfaces are constructed using the $(\varepsilon_{c2o},\varepsilon_{s1})$ criterion for yield and failure, unity safety factors and mean strength values for the materials. Table 5.2 summarizes the material properties and safety factors for the two sections of Fig. 9.

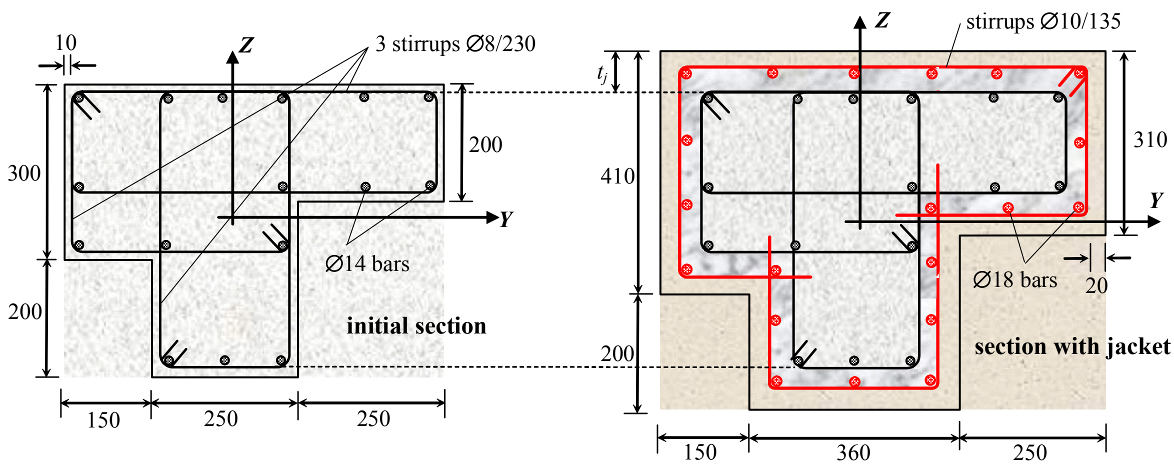

Figure 9. RC T-shaped section with jacket (dimensions in mm).

Table 5.2. Material properties and safety factors for the T-shaped sections of Fig. 9.

Section	f_c (MPa)	β_c	γ_c	ε_{co}	ε_{cu}	z	z^*	$\alpha\omega_w$	E_s (GPa)	f_y (MPa)	γ_s	ε_{su}
Initial	14	1.00	1.00	-0.002	-0.0035	-100	-57.80	0.02	200	220	1.00	0.018
Jacket	22	1.00	1.00	-0.002	-0.0035	-100	-44.73	0.04	200	500	1.00	0.035

In the above table, z^* is the slope of the descending branch of the confined concrete σ-ε law. It is reminded that the criterion (ε_{c2o},ε_{s1}), which is used in the present analysis, corresponds to the yield or failure of the section core. For the case of jacket it is the jacket core. This means that the clear concrete cover of the jacket has been extensively cracked in the yield state or it has been completely removed in the failure state. This is the reason why the failure surface does not completely include the yield surface, as can be seen in Fig. 10(c). Fig. 10(d) shows both surfaces to be fully enclosed if the (ε_{c2},ε_{s1}), criterion is used. Fig. 11 shows similar results for the case of the initial section.

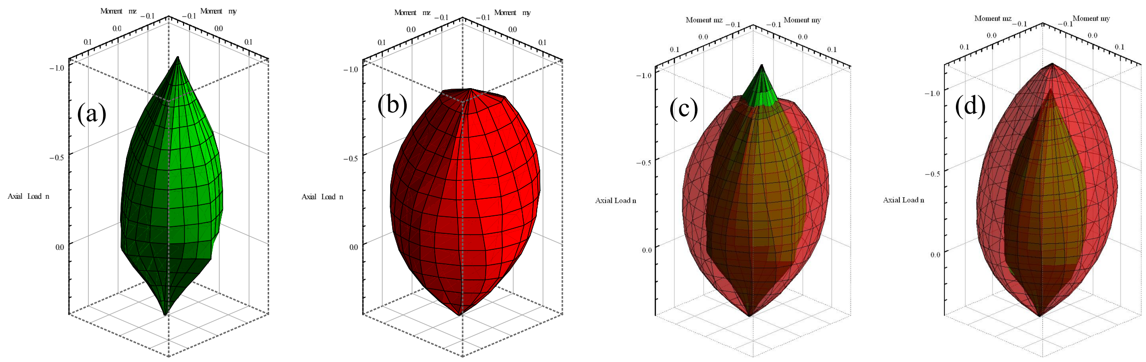

Figure 10. Yield and Failure surfaces of section with jacket: (a) Yield, (b) Failure, (c) and (d) both, enclosed.

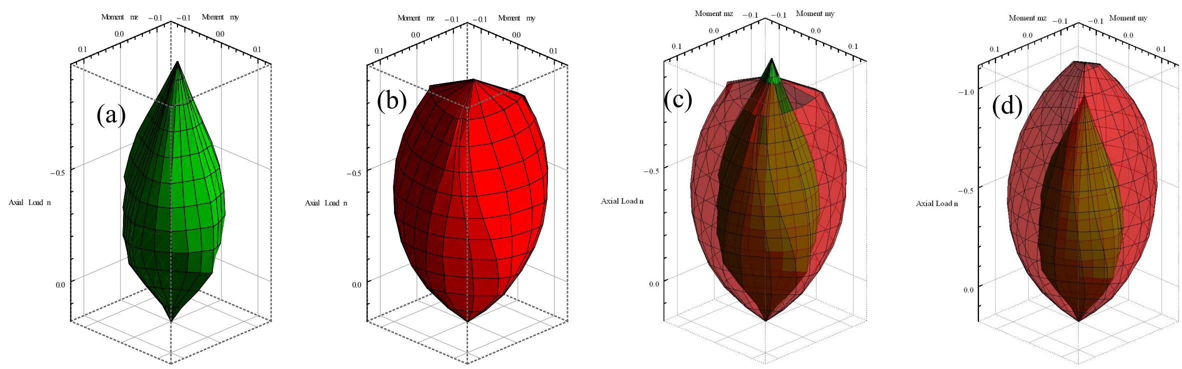

Figure 11. Yield and Failure surfaces of the initial section: (a) Yield, (b) Failure, (c) and (d) both, enclosed.

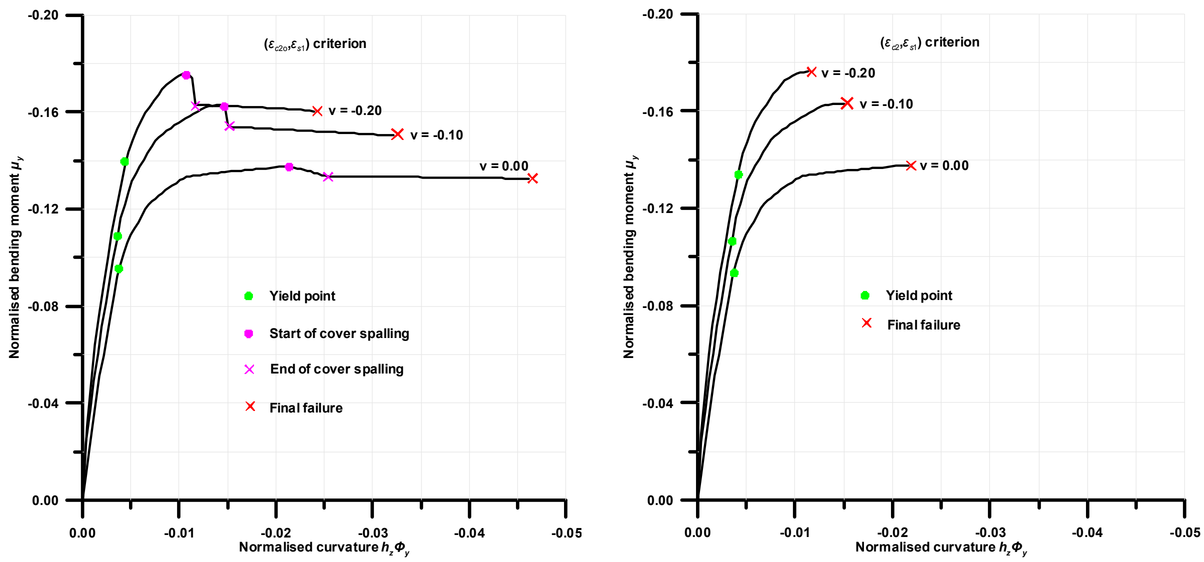

Figure 12. Normalized moment-curvature diagrams for section with jacket.

For all the analyses, the increase of the concrete compressive strength due to confinement has been taken into account by means of the product $\alpha\omega_w$, according to Eurocode 2.
Fig. 12 shows the full moment curvature diagrams for $\theta = 180^o$ and $v = 0.00, -0.10, -0.20$ for both criteria, as they were computed by the model. From these diagrams it is obvious that the size of the failure surface depends on how the final failure is defined, i.e. taking as criterion the concrete cover spalling or the failure of the section core. For purposes of seismic assessment, the second one is more reliable since it affects the real condition of a prismatic RC element.

6. CONCLUSIONS

The present graphic fiber model can analyze any cross sectional shape including the case of composite sections, sections with reinforced concrete jackets and sections with openings. It can incorporate various yield or failure criteria for a RC section, according to the desired purpose. Moreover, one can use any other modified of the stress-strain laws for steel and concrete. Its computer implementation is quite simple so it can be incorporated as a reliable computational tool in any open FEM code. Because of these advantages, it can be successfully used for both the nonlinear analysis of structures, either for design purposes or for seismic assessment and retrofitting of RC structures. Its generality makes it capable for computing more reliably and accurately various parameters needed in nonlinear models, for cases of sections other than the classic orthogonal. In this point it must be noted that for nonclassic section geometries, the use of analytic relations for orthogonal sections is not always a good approximation, so the present computational tool can fill this gap with quite success.

REFERENCES

Al-Noury, S.I. and Chen, W.F. (1982). Behavior and Design of Reinforced and Composite Concrete Sections. *Journal of Structural Division, ASCE* **108:6**, 1266-1284.

Cheng-Tzu and Hsu, T. (1985). Biaxially Loaded L-Shaped Reinforced Concrete Columns. *Journal of Structural Engineering* **111:12**, 2576-2595.

Sousa Jr., J.B.M. and Muniz, C.F.D.G. (2007). Analytical integration of cross section properties for numerical analysis of reinforced concrete, steel and composite frames. *Engineering Structures* **29:4**, 618–625

Charalampakis, A.E. and Koumousis, V.K. (2008). Ultimate strength analysis of composite sections under biaxial bending and axial load. *Advances in Engineering Software* **39:11**, 923-936.

Sfakianakis, M.G. (2002). Biaxial bending with axial force of reinforced, composite and repaired concrete sections of arbitrary shape by fiber model and computer graphics. *Advances in Engineering Software* **33:4**, 227-242.

Eurocode 2 (2005). Design of concrete structures - Part 1-1: General rules and rules for buildings, ΕΛΟΤ EN 1992-1-1 (in Greek).

Fardis, M.N., (2009). Seismic Design, Assessment and Retrofitting of Concrete Buildings. Springer ed.

FEMA 356 (2000). Prestandard and Commentary for the Seismic Rehabilitation of Buildings. ASCE.

Greek Code for Reinforced Concrete (2004). ΕΚΩΣ 2000 (in Greek).

Greek Code for Assessment and Retrofitting of Reinforced Concrete Structures (2012). ΚΑΝ.ΕΠΕ. 2012 (in Greek).

Old Greek National Code for Seismic Actions (1959). (In Greek).